First publ. in: Journal of Applied Physics 99 (2006), 033904

Structure-induced magnetic anisotropy in the Fe(110)/Mo(110)/$Al_2O_3(11\bar{2}0)$ system

M. Fraune,[a] J. O. Hauch, and G. Güntherodt
II. Physikalisches Institut, Rheinisch-Westfälische Technische Hochschule Aachen, 52056 Aachen, Germany

M. Laufenberg, M. Fonin, and U. Rüdiger
Fachbereich Physik, Universität Konstanz, 78457 Konstanz, Germany

J. Mayer
Gemeinschaftslabor für Elektronenmikroskopie, Rheinisch-Westfälische Technische Hochschule Aachen, 52056 Aachen, Germany

P. Turban
Laboratoire PALMS Groupe Surfaces et Interfaces Université de Rennes I, Campus de Beaulieu, 35042 Rennes Cedex, France

Fe(110) films were epitaxially grown on sapphire substrates using a Mo(110) buffer layer in an ultrahigh-vacuum molecular-beam epitaxy system. The magnetic properties were examined *ex situ* by Brillouin light scattering and superconducting quantum interference device magnetometry. To determine the magnetic anisotropy constants the frequency of the Damon-Eshbach [J. Phys. Chem. Solids **19**, 308 (1961)] surface spin-wave mode was measured as a function of the in-plane angle between the external magnetic field and the Fe[001] crystal axis. The angle-dependent frequency was fitted by a spin-wave model. We found that the easy axis of the cubic magnetocrystalline anisotropy K_1 and an additional uniaxial in-plane anisotropy $K_{\parallel}^{(2)}$ are aligned parallel to the in-plane Fe[001] axis for Fe-layer thicknesses from 0.8 to 37 nm, with K_1 increasing and $K_{\parallel}^{(2)}$ decreasing with increasing Fe thickness. Possible origins of the observed uniaxial anisotropy are discussed.

I. INTRODUCTION

Research in the field of thin-film magnetism has attracted increasing interest during the last decade due to its impact on applications, e.g., in storage and sensor technology. Based on the discovery of giant magnetoresistance[1,2] (GMR) as well as tunneling magnetoresistance (TMR),[3] a concept for a nonvolatile magnetic random access memory (MRAM) has been developed.[4–6] For this purpose reproducible and tunable magnetic characteristics and high TMR values are crucial. Especially the uniformity of the switching field of magnetic sensing layers is critical and decisive whether MRAM is a technology applicable for mass production. Therefore, detailed micromagnetic studies are of particular importance for tailoring the magnetic properties of such MRAM cells. This includes experiments on the magnetic switching[7,8] as well as micromagnetic simulations.[9,10] In this context a precise knowledge of magnetic anisotropy energies of the magnetic layers is of outstanding interest.

In this article we focus on epitaxial Fe(110) films of different thicknesses grown on an $Al_2O_3(11\bar{2}0)$ substrate with a Mo(110) buffer layer. The study of epitaxial Fe(110) thin films is motivated by the high spin-polarization value of −80% at E_F at room temperature,[11,12] making it a promising material to be used in magnetic tunnel junctions. The epitaxial growth of this system has already been studied in detail.[13–18] It turned out that the misfit of about 8.9% between the Fe and the Mo lattices leads to a lattice strain that is released by dislocations ordered in lines.[16] *In situ* grazing incidence x-ray scattering (GIXS) and calculations using elasticity theory predict a thickness-dependent uniaxial magnetic anisotropy with a [001] easy axis due to the relaxing strain.[13]

The relevant magnetic anisotropy energies of our Fe(110) films have been investigated by Brillouin light-scattering (BLS) measurements of spin waves, using appropriate fitting algorithms. Here, these anisotropies are, in particular, the first-order cubic anisotropy K_1, a uniaxial in-plane anisotropy $K_{\parallel}^{(2)}$, and to some extent a uniaxial out-of-plane anisotropy $K_{\perp}^{(2)}$. To complement previous studies on the magnetism of the Fe/Mo system,[13,15,18] detailed angular scans of the applied in-plane magnetic field were performed using a fully automated setup. Thus the angular dependence of the spin-wave frequency reveals the exact position of the easy and hard axes present in the system. As the samples were always magnetically saturated during the measurements, the influence of the particular magnetization reversal mechanisms such as domain-wall nucleation, pinning, and propagation could be eliminated. These partially extrinsic effects might complicate the analysis of the anisotropy constants when a nonuniformly magnetized sample is probed only locally, for instance, in magneto-optical Kerr effect (MOKE) hysteresis measurements.

[a]Electronic mail: fraune@physik.rwth-aachen.de

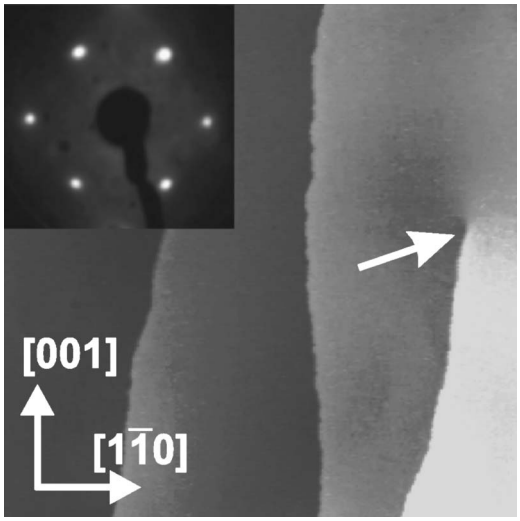

FIG. 1. 100×100 nm^2 STM image of a 20-nm-thick Fe(110) film deposited on the Mo(110)/$Al_2O_3(11\bar{2}0)$ system at RT and subsequently annealed at 800 K. The inset shows a LEED pattern of the same film. The white arrow marks a screw dislocation.

II. SAMPLE PREPARATION

The films were grown on 5×10 mm^2 $Al_2O_3(11\bar{2}0)$ substrates by molecular-beam epitaxy (MBE) in an ultrahigh-vacuum (UHV) system. The Mo buffer layer was deposited at 1000 K with a thickness of 20 nm. Different samples were prepared with Fe thicknesses of 0.8, 1.2, 2.9, 6.1, 15.3, 17.2, and 37.0 nm deposited at room temperature (RT), and subsequently annealed at 800 K. An aluminum cap layer of 3 nm was grown on top to prevent oxidation of the Fe films during the *ex situ* experiments using BLS and super conducting quantum interference device (SQUID) measurements. Reflection high-energy electron diffraction (RHEED) was used to control the growth process. The layer thickness was measured by means of a quartz microbalance with an accuracy of ±10%, and cross-checked by SQUID magnetometry.

Further details about the preparation conditions of our samples are given in Refs. 16 and 17.

III. SAMPLE CHARACTERIZATION

In order to investigate the surface morphology of the Mo and Fe layers, a 20-nm-thick reference sample was grown in a MBE setup equipped with *in situ* scanning tunneling microscopy (STM) and low-energy electron diffraction (LEED). A STM image of the Fe(110) surface is shown in Fig. 1. Monoatomic terraces with a width of several tens of nanometers can be observed with their edges aligned preferentially along the in-plane Fe[001] axis. The origin of this step formation is attributed to a slight unintended miscut of less than 0.3° of the Al_2O_3 substrate. The white arrow marks a screw dislocation. A very sharp (1×1) LEED pattern of the bcc Fe(110) surface with a typical twofold symmetry is shown in the inset of Fig. 1. Figure 2 shows a high-resolution cross-sectional transmission electron microscopy (TEM) image of a reference sample with a 7-nm-thick Mo buffer layer. The image was taken along the [001] zone axis of the Fe and the Mo lattices. The expected lattice symmetries are clearly visible in the substrate, the Mo buffer and the Fe layer. A local chemical analysis using electron-energy-loss spectroscopy (EELS) did not reveal any interdiffusion of Fe or Mo atoms.

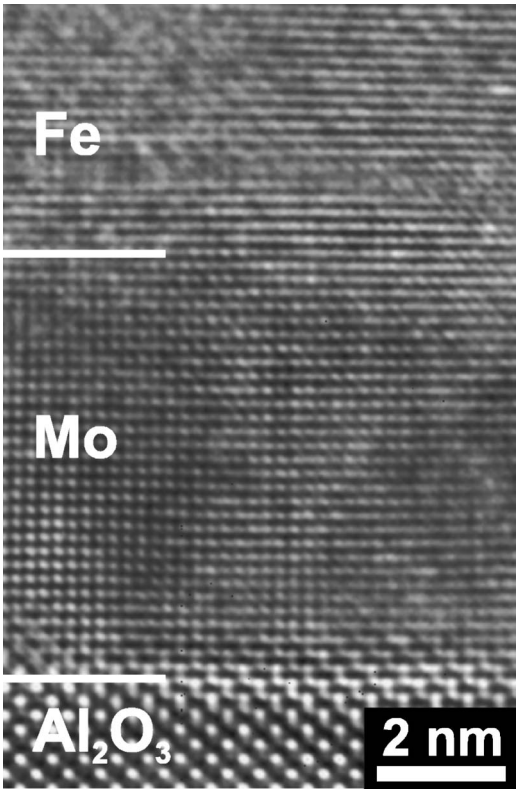

FIG. 2. High-resolution cross-sectional TEM micrograph of the Fe(110)/Mo(110) layer system on an $Al_2O_3(11\bar{2}0)$ substrate. The positions of the interfaces are marked by white lines. The image was taken along the in-plane [001] zone axis, which was verified by evaluating electron-diffraction patterns.

SQUID magnetometry was carried out along the [001] and [1$\bar{1}$0] in-plane directions. Hence the magnetic saturation fields of the samples were determined to ensure saturation during the BLS measurements. The measured saturation moments were used to check the thickness of the Fe layers determined by the quartz microbalance. This method is appropriate because the volume magnetization is constant and equal to the bulk value of $M_S=(1.71\pm0.01)\times10^6$ A/m in the thickness range of our samples.[19]

The hysteresis loops of a 1.2-nm-thick Fe layer in Fig. 3 show that the magnetic easy axis lies along the in-plane [001] direction and the hard axis along the [1$\bar{1}$0] direction. The saturation fields of 90 mT for the easy and 140 mT for the hard axis are small enough to provide saturation during the BLS measurements which were performed at 300 mT for the 1.2-nm-thick sample and at 200 mT for all other samples.

IV. EXPERIMENTAL RESULTS AND DISCUSSION

BLS experiments were carried out at room temperature to study the spin-wave frequency of the Damon-Eshbach mode[20] as a function of the Fe layer thickness and the in-plane direction of the applied magnetic field. Linearly polarized light of a single-mode Ar^+-ion laser with a wavelength

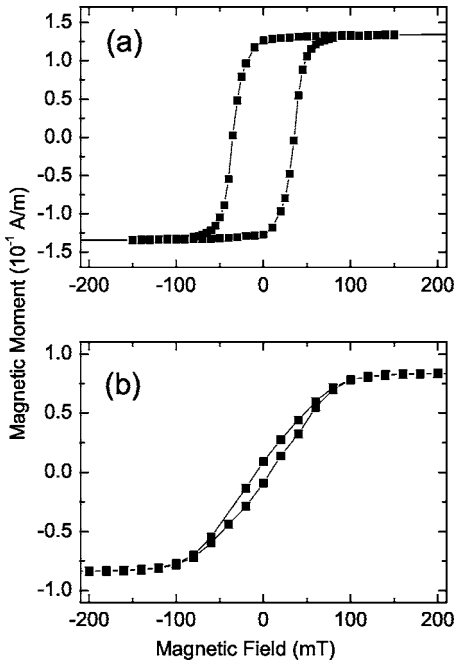

FIG. 3. SQUID hysteresis loop measurements of 1.2 nm Fe(110) on $Mo(110)/Al_2O_3(11\bar{2}0)$ with the magnetic field applied along (a) the in-plane [001] direction and (b) the in-plane $[1\bar{1}0]$ direction.

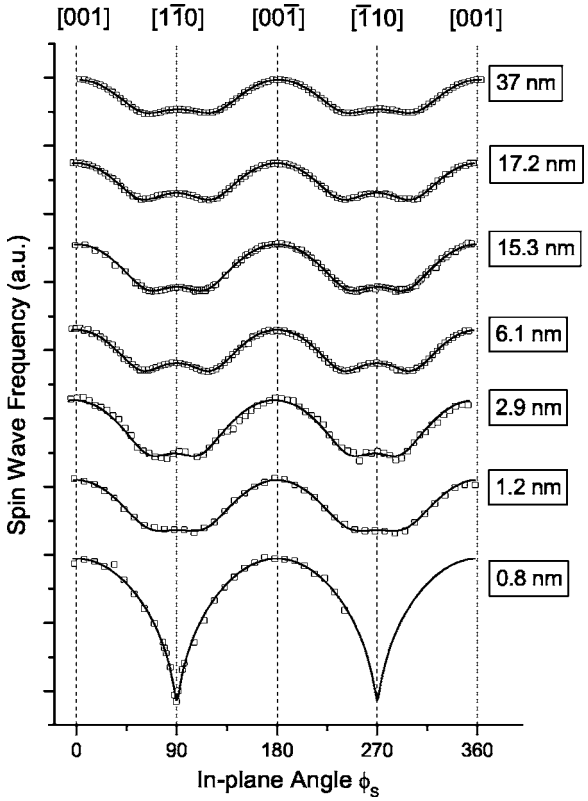

FIG. 4. Frequencies of the Damon-Eshbach mode as a function of the in-plane rotation angle ϕ_S for different thicknesses of the Fe film. ϕ_S is measured between the external field and the Fe [001] axis. The solid lines are obtained by fitting the data as described in Sec. IV. The curves are offset for clarity.

of $\lambda = 514.5$ nm is focused in a spot of about 50 μm in diameter on the sample with an incident power of up to 100 mW. In backscattering geometry the angle of incidence $\delta = 45°$ results in a transferred in-plane wave vector of $k_\parallel = 1.727 \times 10^7$ m^{-1}. The light is inelastically scattered by thermally excited spin waves and analyzed by a fully automated Sandercock triple pass tandem Fabry-Pérot[21] (TFP) interferometer using a photomultiplier tube. Phonon-generated signals are eliminated by light polarization analysis.

A constant external magnetic field is applied in the sample plane and perpendicular to the incident photon wave vector. The sample plane can be rotated about its normal by means of a stepper motor so that the angle ϕ_S between a given in-plane crystal axis and the applied magnetic field can be varied between 0° and 360°. For each sample a rotational scan of the spin-wave spectra is taken by varying ϕ_S. The accumulation time for one spectrum varies significantly between approximately 15 min for the thickest films up to more than 3 h for the 0.8-nm-thick film.

The frequencies of the Damon-Eshbach mode peaks in the collected spectra were determined by a multiparameter least-squares fit with a sixth-power Lorentzian function. The corresponding error is less than ±0.2 GHz. The frequencies shift significantly with the rotation angle ϕ_S. High and low frequencies can be attributed to the easy and hard magnetic axes, respectively. As shown in Fig. 4, a strong thickness dependence of the frequency versus in-plane field-angle curve can be observed, which is directly related to a dramatic change in the magnetic anisotropies of the Fe films. In order to extract the anisotropy constants, the angle-dependent spin-wave frequencies were fitted using an appropriate spin-wave model[22] and the following free-energy density:

$$F_{\text{ani}} = \frac{K_1}{4}[\sin^4 \phi_S + \sin^2(2\phi_S)] + K_\parallel^{(2)} \cos^2 \phi_S \sin \theta_M + K_\perp^{(2)} \cos^2 \theta_M. \quad (1)$$

Here, K_1 denotes the magnetocrystalline anisotropy constant of the cubic Fe lattice, $K_\parallel^{(2)}$ a uniaxial (twofold) in-plane anisotropy, and $K_\perp^{(2)}$ a uniaxial out-of-plane anisotropy. The latter was not evaluated in this study, because it does not influence the in-plane anisotropy constants, but rather results in a constant offset in spin-wave frequency for all in-plane angles. For the given thicknesses $K_\perp^{(2)}$ is always negative and the film plane is an easy plane of magnetization. ϕ_S is the angle between the in-plane [001] direction and the applied magnetic field, and θ_M the out-of-plane polar angle of the magnetization M.

The fit curves are plotted as solid liens in Fig. 4. Note that a considerable part of the uniaxial character of all curves is generated by the twofold symmetry of the (110) surface and is included in K_1. This bulk magnetocrystalline contribution also accounts for the effect that for thick films there is not one single magnetic hard axis aligned along $[1\bar{1}0]$ but rather two equivalent hard axes (frequency minima) shifted about 25° to both sides of the $[1\bar{1}0]$ axis. Yet even in the thickest film of 37 nm in thickness this shift does not reach the 35.26° shift that would correspond to the in-plane $[1\bar{1}0]$ or $[\bar{1}11]$ axes which represent the hard magnetocrystalline axes in bulk Fe single crystals. The small local maximum at

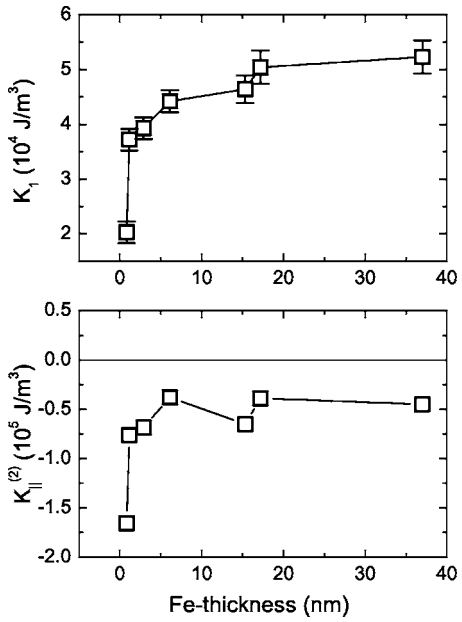

FIG. 5. Anisotropy constants K_1 and $K_{\parallel}^{(2)}$ for Fe(110) films of different thicknesses on a Mo(110)-buffer layer. The errors in K_1 are calculated from estimated deviations of 10% in thickness and in magnetic field. For $K_{\parallel}^{(2)}$ they are smaller than the symbol size.

90° (i.e., with the field parallel to the $[1\bar{1}0]$ direction) for thicknesses $\geqslant$2.9 nm is thus given by the superposition of the easy magnetocrystalline axes lying parallel to the [100] and $[0\bar{1}0]$ directions which point 45° out of the film plane. Correspondingly the local maximum at 270° (i.e., with the field parallel to $[\bar{1}10]$) is given by the superposition of the easy axes lying parallel to $[\bar{1}00]$ and [010]. These local maxima are suppressed for the thinnest film, where the uniaxial contribution of $K_{\parallel}^{(2)}$ prevails. As the local maxima in spin-wave frequency correspond to local minima in the free-energy density F_{ani}, their suppression for the two thinnest films of 0.8 and 1.2 nm in thickness implies the suppression of possible metastable states of magnetization parallel to the $[1\bar{1}0]$ or $[\bar{1}10]$ axis. This is particularly intriguing with regard to possible applications of Fe(110) in magnetic memory or sensing devices, where the magnetization of magnetoresistive electrodes in memory cells or sensors has to be uniform and aligned along a well-defined axis.

The quantitative dependence of the anisotropy constants on the Fe-film thickness is shown in Fig. 5. The value of K_1 is smallest for the thinnest film of 0.8 nm, strongly increases for 1.2 nm, and then grows monotonically with increasing film thickness, approaching a limit of about $(5.2\pm0.3)\times10^4$ J/m^3, which is slightly larger than the value of 4.8×10^4 J/m^3 known from the literature.[23] In the 0.8-nm film, nominally consisting of four monolayers, only the two inner layers, i.e., half of the material, are surrounded by a bcc-like symmetry. Therefore the strong reduction of magnetocrystalline anisotropy in this film can be attributed to the loss of bulk crystalline symmetry.

The uniaxial in-plane anisotropy constant $K_{\parallel}^{(2)}$ shows a completely different thickness dependence. This contribution is strongest for the thinnest film and abruptly decreases with increasing thickness to a value of $(-0.5\pm0.5)\times10^5$ J/m^3 at which it levels off for further increasing Fe layer thickness. The negative sign of $K_{\parallel}^{(2)}$ for all measured thicknesses indicates an easy axis in plane and parallel to the easy axis of the magnetocrystalline anisotropy K_1. This has already been observed in earlier studies[15] and is contrary to the case of Fe(110) on W(110), where the magnetic easy axis switches to the in-plane $[1\bar{1}0]$ direction for film thicknesses below 9.5 nm.[24] The reason for these different behaviors of the uniaxial anisotropy in Fe(110)/W(110) and Fe(110)/Mo(110) is still controversial.

A number of possible origins of the uniaxial anisotropy exist: Néel-type surface anisotropy,[25] step edge anisotropy induced by a miscut of the sapphire substrate, magnetoelastic anisotropy caused by the lattice mismatch of 8.9% at the Fe/Mo interface, or dislocations that enter the Fe film during strain relaxation.[13,14] The first two effects show an inverse thickness dependence, because they are induced by the interface itself. Furthermore, Usov *et al.*[18] have shown that steps aligned perpendicular to the in-plane $[1\bar{1}\bar{1}]$ direction, with a step density more than ten times higher than in our samples, only cause a small deviation of the easy axis from the [001] direction, and the effect levels off for film thicknesses above 1.2 nm. If we suppose that a step along [001], like in our samples, does not induce a considerably larger amount of anisotropy energy than a differently aligned step, then the steps alone can neither be responsible for the strong increase of the uniaxial anisotropy in our thinnest films nor for the residual uniaxial magnetic anisotropy at higher thicknesses. In contrast, strain and magnetostriction may affect more than the interfacial layers and can be reduced by dislocations, producing a more complicated thickness dependence.[13] Dislocations were shown to appear in a hexagonal network.[14] If these dislocations were directly related to the magnetic anisotropy, their hexagonal alignment should be reflected in the symmetry of the anisotropy. This was not observed. As the measured uniaxial anisotropy in our samples converges to a constant value of about -0.5×10^4 J/m^3 for thicknesses above 5 nm, we infer that purely interface-related effects cannot be solely responsible for the observed behavior. Films of 37 nm in thickness may still exhibit a strain of the order of 1% (Ref. 13) and STM images of dislocations in 20-mn-thick films (see Fig. 1) show that even at these comparably large thicknesses the strain has not completely relaxed. Therefore the anisotropic strain relaxation observed by Clemens *et al.*[13] appears to be the origin of the strongly increased uniaxial magnetic anisotropy. Their calculated anisotropy energies are comparable in magnitude to our measured values, although the thickness dependence is slightly different, which may be caused by differences in the preparation conditions.

Controlling the strain-induced anisotropy by modifying the growth and the annealing process might therefore make it possible to induce a pure uniaxial anisotropy and to suppress the local minima in the angle-dependent free energy (the maxima in spin-wave frequency) at 90° and 270° even for films thicker than 3 nm. This could be of interest in applica-

tions where a strong uniaxial anisotropy is needed and where it is impossible to influence the anisotropy by other means, for instance, by the shape anisotropy.

V. CONCLUSION

In conclusion, we have prepared epitaxial Fe(110) layers of different thicknesses on sapphire substrates using a Mo(110) buffer layer. The magnetic anisotropy contributions have been measured by SQUID and BLS. The magnetocrystalline anisotropy K_1 builds up rapidly with increasing Fe layer thickness to stabilize slightly above the value measured in bulk single crystals. An in-plane uniaxial anisotropy contribution $K_{\parallel}^{(2)}$ favors the [001] easy axis at all measured thicknesses. Contrary to previous studies in similar systems,[15] it does not go to zero even at the largest measured thickness of 37 nm. Anisotropic relaxation of the strain induced by the lattice mismatch at the Fe/Mo interface is made responsible for this effect. This finding is consistent with the conclusions by Clemens *et al.*[13]

ACKNOWLEDGMENT

We would like to thank B. Hillebrands for help with the fitting procedure.

[1]M. N. Baibich *et al.*, Phys. Rev. Lett. **61**, 2472 (1988).
[2]G. Binasch, P. Grünberg, F. Saurenbach, and W. Zinn, Phys. Rev. B **39**, 4828 (1989).
[3]J. S. Moodera, L. R. Kinder, T. M. Wong, and R. Meservey, Phys. Rev. Lett. **74**, 3273 (1995).
[4]W. J. Gallaghen, *et al.* J. Appl. Phys. **81**, 3741 (1997).
[5]J. M. Daughton, J. Appl. Phys. **81**, 3758 (1997).
[6]S. S. P. Parkin, *et al.* J. Appl. Phys. **85**, 5828 (1999).
[7]K. J. Kirk, J. N. Chapman, and C. D. W. Wilkinson, Appl. Phys. Lett. **71**, 539 (1997).
[8]J. Yu, U. Rüdiger, A. D. Kent, L. Thomas, and S. S. P. Parkin, Phys. Rev. B **60**, 7352 (1999).
[9]T. Schrefl, J. Fidler, K. J. Kirk, and J. N. Chapman, J. Magn. Magn. Mater. **175**, 193 (1997).
[10]C. König, *et al.* Appl. Phys. Lett. **79**, 3648 (2001).
[11]R. Kurzawa, K.-P. Kämper, W. Schmitt, and G. Güntherodt, Solid State Commun. **60**, 777 (1986).
[12]Y. S. Dedkov, M. Fonin, U. Rüdiger, and G. Güntherodt, Appl. Phys. Lett. **81**, 2584 (2002).
[13]B. M. Clemens, R. Osgood, A. P. Payne, B. M. Lairson, S. Brennan, R. L. White, and W. D. Nix, J. Magn. Magn. Mater. **121**, 37 (1993).
[14]J. Malzbender, M. Przybylski, J. Giergiel, and J. Kirschner, Surf. Sci. **414**, 187 (1998).
[15]O. Fruchart, J. P. Nozières, and D. Givord, J. Magn. Magn. Mater. **207**, 158 (1999).
[16]U. May, R. Calarco, J. O. Hauch, H. Kittur, M. Fonine, U. Rüdiger, and G. Güntherodt, Surf. Sci. **489**, 144 (2001).
[17]M. Fonin, Y. S. Dedkov, J. Mayer, U. Rüdiger, and G. Güntherodt, Phys. Rev. B **68**, 045414 (2003).
[18]V. Usov, S. Murphy, and I. V. Shvets, J. Appl. Phys. **95**, 7312 (2004).
[19]U. Gradmann, in *Handbook of Magnetic Materials*, edited by K. H. J. Buschow (North-Holland, Amsterdam, 1993).
[20]R. W. Damon and J. R. Eshbach, J. Phys. Chem. Solids **19**, 308 (1961).
[21]B. Hillebrands, Rev. Sci. Instrum. **70**, 1589 (1999).
[22]R. L. Stamps and B. Hillebrands, Phys. Rev. B **44**, 12417 (1991).
[23]S. D. Hanham, A. S. Arrott, and B. Heinrich, J. Appl. Phys. **52**, 1941 (1981), cited in Landolt-Börnstein, New Series III/19a.
[24]B. Hillebrands, P. Baumgart, and G. Güntherodt, Phys. Rev. B **36**, 2450 (1987).
[25]L. Néel, J. Phys. Radium **15**, 225 (1954).